Received: 2 December 2021 | Revised: 8 February 2022 | Accepted: 29 March 2022

DOI: 10.1002/sia.7097

RESEARCH ARTICLE

SURFACE and INTERFACE ANALYSIS WILEY

Monitoring electrode/electrolyte interfaces of Li-ion batteries under working conditions: A surface-enhanced Raman spectroscopic study on $LiCoO_2$ composite cathodes

Marcel Heber | Christian Hess

Eduard-Zintl-Institute of Inorganic and Physical Chemistry, Technical University of Darmstadt, Darmstadt, Germany

Correspondence
Christian Hess, Eduard-Zintl-Institute of Inorganic and Physical Chemistry, Technical University of Darmstadt, Alarich-Weiss-Str. 8, 64287 Darmstadt, Germany.
Email: christian.hess@tu-darmstadt.de

Funding information
Deutsche Forschungsgemeinschaft, Grant/Award Number: HE 4515/8-1; Technische Universität Darmstadt

Lithium-ion batteries are commonly used for electrical energy storage in portable devices and are promising systems for large-scale energy storage. However, their application is still limited due to electrode degradation and stability issues. To enhance the fundamental understanding of electrode degradation, we report on the Raman spectroscopic characterization of $LiCoO_2$ cathode materials of working Li-ion batteries. To facilitate the spectroscopic analysis of the solid electrolyte interface (SEI), we apply in situ surface-enhanced Raman spectroscopy under battery working conditions by using Au nanoparticles coated with a thin SiO_2 layer ($Au@SiO_2$). We observe a surface-enhanced Raman signal of Li_2CO_3 at 1090 cm^{-1} during electrochemical cycling as an intermediate. Its formation/decomposition highlights the role of Li_2CO_3 as a component of the SEI on $LiCoO_2$ composite cathodes. Our results demonstrate the potential of Raman spectroscopy to monitor electrode/electrolyte interfaces of lithium-ion batteries under working conditions thus allowing relations between electrochemical performance and structural changes to be established.

KEYWORDS
in situ spectroscopy, $LiCoO_2$, lithium batteries, Raman spectroscopy, SERS, SHINERS, solid electrolyte interface

1 | INTRODUCTION

In light of the climate change and scarcity of fossil fuels, the topic of sustainable energy production and their usage becomes more and more relevant. In addition to the use of renewable energy sources, the storage of energy and the conversion of the transportation industry to electric vehicles represent important challenges for today's research, in which batteries play a key role. Among the rechargeable batteries, especially the lithium-ion battery is used in electronic devices.[1] The commercial lithium-ion battery contains, for example, $LiCoO_2$ as cathode material. Advantages of $LiCoO_2$ are its high specific capacity, low self-discharge, and high cycle life.[2] During the initial charging and discharging processes of the lithium-ion battery, a coating layer (SEI = solid electrolyte interface) forms on the electrode surface due to the reaction between the electrolyte and the cathode material, which may influence the capacity and life time of the battery.[1,3] A detailed characterization of the composition and formation processes of the top layer is therefore essential for the efficient use of lithium-ion batteries.[4,5] This layer is permeable to lithium ions and causes passivation of the electrode material,[1] protecting it against further surface reactions and dendrite formation.[6] However, due to the formation of the SEI, some of the lithium ions are irreversibly lost. Furthermore, it represents an additional diffusion resistance, which can be speed determining depending on the ion conductivity of the formed layer.[7] Reports on the chemical composition of the SEI include inorganic compounds such as Li_2O, LiF, and Li_2CO_3[5,6] and organic

compounds such as $ROCO_2Li$, ROLi, and LiOH.[5,8–12] There are several ex situ but only few in situ techniques available to study the electrode/electrolyte interface,[5] such as X-ray reflectometry (XRR), neutron reflectometry (NR), and surface-enhanced Raman spectroscopy (SERS).[5,9,12] For the characterization of the electrode material, Raman spectroscopy has proved to be a powerful method, as it can be performed without specific sample preparation and is suitable for in situ measurements,[5,13] thus allowing to monitor the dynamics inside the active material during the electrochemical process and to establish relations between electrochemical performance and structural changes. The literature describes a high temperature (HT) and a low temperature (LT) phase of $LiCoO_2$. In this study, HT-$LiCoO_2$ is used as a cathode material, which crystallizes in a hexagonal layer structure (space group $R\bar{3}m$),[14] consisting of a close-packed network of oxygen atoms with the Li^+ and Co^{3+} ions ordering on alternating (111) planes of the cubic rock-salt structure.[15] According to its space group, the irreducible representation is $A_{1g} + 2A_{2u} + E_g + 2E_u$, and the odd vibrational modes are Raman inactive, while the straight modes are Raman active (A_{1g} and E_g).[13] The first Raman study on $LiCoO_2$ was reported by Inaba et al.,[16] in which the effect of the lithium content on the Raman-active bands was investigated, showing a reduction of the signal intensity due to deintercalation.[16] A disadvantage of normal Raman spectroscopy is its low sensitivity, which makes detection of the SEI layer difficult.[17] However, this issue can be resolved by using SERS,[18] which provides a signal enhancement of up to six orders of magnitude[19] near rough Au, Ag, or Cu surfaces,[17] and has enabled identification of chemical species and detailed structural characterization in various research fields, including materials science, biosensing, catalysis, and electrochemistry.[20] Electrochemical electrodes are typically metal surfaces, allowing the direct application of SERS to study the behavior of adsorbed molecules,[20–24] such as tetrathiafulvalene (TTF) derivatives extensively used in mechanostereochemistry and molecular electronic devices.[20–22] Using SHINERS, the SERS effect can be transferred to any sample surface, by coating metal nanoparticles with an inert shell such as SiO_2 or Al_2O_3.[25] In the context of lithium-ion battery materials, such a SERS-based approach has been applied previously to lithium-rich cathode and Si anode materials.[26,27] Hy et al. applied this approach to surface reactions on lithium-rich cathode materials ($Li[Ni_xLi_{(1-2x)/3}Mn_{(2-x)/3}]O_2$, $0 \le x \le 0.5$) during electrochemical cycling, and reported on the detection of intermediately formed Li_2O, leading to Li_2CO_3 as a result of decomposition reactions of the electrolyte at the cathode.[26] Teshager et al. examined layered (lithium-rich) $Li_{1.2}Ni_{0.2}Mn_{0.6}O_2$ (LLNMO) and $LiCoO_2$ cathodes during first- and second-cycle charging and discharging with diffuse reflectance infrared Fourier-transformed spectroscopy (DRIFTS) while circulating the electrolyte.[28] This raises the question whether the conditions under electrolyte circulation can be compared with those of a conventional battery under working conditions. The authors reported various SEI species, for example, RCOOR, Li_2CO_3, and $ROCO_2Li$, during charging above 4.0 and 4.5 V and during discharging below 3.6 and 4.0 V for $LiCoO_2$ and LLNMO, respectively, attributed to EC decomposition.[28] In the context of Li-ion and Li-O_2 cells, Galloway et al. observed the formation of LiO_2, Li_2O_2, and Li_2CO_3 on lithium metal and planar carbon electrode interfaces, as well as on composite carbon black electrodes.[29]

In this study, we use SERS to study $LiCoO_2$ composite cathodes during electrochemical cycling. First, the synthesis and characterization of the shell-isolated Au@SiO_2 nanoparticles is presented. We then apply the nanoparticles to $LiCoO_2$ composite cathodes, allowing us to identify chemical species of the SEI layer and to monitor their dynamic behavior during electrochemical cycling.

2 | EXPERIMENTAL SECTION

2.1 | Synthesis of the composite cathode

The synthesis of $LiCoO_2$ follows the Pechini process, which ensures a statistical distribution of the cations in the material.[30] $LiNO_3$ (Merck KGaA, ≥98%), $Co(NO_3)_2$ * $6H_2O$ (Merck KGaA, ≥99.0%), and citric acid (AppliChem, ≥98%) are weighted and dissolved in water. A concentrated ammonia solution (25%) is then added dropwise to the solution until the pH value is adjusted to 5. Ethylene glycol is added into the suspension and the temperature is set to 180°C for 6 h. The resulting black solid is first collected and ground and then precalcined at 450°C for 6 h (heating rate: 1.5°C/min). The obtained brown powder is ground und calcined at 800°C for 25 h (heating rate: 20°C/min).

For the preparation of the composite cathode, the obtained $LiCoO_2$ is mixed with carbon black (TIMCAL, super p) and polyvinylidene fluoride (PVDF, Solef, 6020/1001 H-6091) with a weight ratio of 84:8:8. By adding *N*-methyl-2-pyrrolidone (NMP) dropwise into the mixture, a thick flowing slurry is formed, which is then brushed on an aluminum net and dried overnight. The final material is cut into 12 mm round plates for insertion into the test cell. As discussed previously, the size of the individual active mass particles varies within 10–20 μm.[31]

2.2 | Synthesis of Au@SiO_2

An aqueous solution of gold chloric acid ($HAuCl_4 \cdot 3H_2O$, Sigma-Aldrich, ≥99.9%) is refluxed in a three-necked flask. To the boiling solution 3% TSC ($Na_3C_6H_5O_7$ * $2H_2O$, Sigma-Aldrich, ≥99.9%) solution is added and stirred for further 15 min under reflux. Then, the solution is cooled to room temperature. Polyvinylpyrrolidone (PVP, Sigma-Aldrich, MW = 40,000 g/mol) solution at a concentration of 12.8 mg/ml is added and stirred at room temperature overnight. After centrifuging, the sample is dispersed in water. The gold nanoparticles (AuNP) solution is added rapidly to a solution of anhydrous ethanol (Sigma-Aldrich, ≥99.8%), water, and 25 wt% NH_4OH solution.

For the preparation of coated AuNP (Au@SiO_2), 2.5 to 50 μl tetraethyl orthosilicate (TEOS, Sigma-Aldrich, ≥98%) in anhydrous ethanol is added to the solution. The solution is stirred for 4 h at room temperature and then centrifuged. The residue is washed three times with anhydrous ethanol. After each washing step, the solution is centrifuged again. The residue is dispersed in water.

2.3 | Characterization of Au@SiO_2

The coated nanoparticles were checked for conformity by the gold-catalyzed reduction of *p*-nitrophenol as an integral probe.[32] To this end, water, $NaBH_4$-solution (Merck), and 0.01 M *p*-nitrophenol are mixed in a cuvette. To this mixture, 100 µl of the nanoparticle solution is added and monitored by UV–VIS spectroscopy (Jasco V-770).

2.4 | Raman spectroscopy

Raman experiments were performed by using 632 nm laser excitation from a diode laser (Ondax). The scattered light was sent to a transmission spectrometer (Kaiser Optical, HL5R) equipped with an electrically cooled CCD detector with 256×1024 pixels. The elastically scattered light was blocked by SuperNotch Plus filters (Kaiser Optical). For the calibration of the spectrometer, emission lines of a standard Ne lamp were used. The spectral resolution was 5 cm^{-1}; the wavelength stability was better than 0.5 cm^{-1}. The laser power was set to 3.8 mW as measured at the position of the sample with a power meter (Ophir). The acquisition time for a single spectrum was 240 s, including the application of a cosmic ray filter and subtraction of the dark spectrum (laser off).

In situ Raman experiments were performed in a 180° backscattering geometry using a commercial test cell (EL Cell)[33] equipped with a glass optical window (see Figure 1). The battery cell consists of two electrodes separated by a layer of glass fiber filter paper soaked with electrolyte to prevent a short circuit.

Cyclovoltammetric (CV) cycling was performed using a potentiostat from BioLogic (VSP). Metallic Li served as counter electrode at a cycling rate of 0.3 mV/s using potential limits of $E_{min} = 3.2$ V and $E_{max} = 4.2$ V. The electrolyte LP30 (Sigma-Aldrich, battery grade, impurities: <50 ppm in HF, <15 ppm H_2O) consisted of 1 M $LiPF_6$ dissolved in ethylene carbonate and dimethyl carbonate (ratio 1:1). Comparison of cyclovoltamograms (CVs) obtained for $LiCoO_2$ composite cathodes with and without Au@SiO_2 particles gave no significant difference in the profile of the CVs and therefore no indication for an influence of the Au@SiO_2 particles on the electrochemical behavior.

Raman spectra under quasi in situ conditions were recorded after completing six charging/discharging cycles. In situ Raman spectra were recorded continuously every 4 min during electrochemical cycling, as indicated in Figure 1. The CV profile of the in situ experiment is shown in Figure S1. The test cell used for all Raman experiments made no observable contribution to the Raman signal. As part of the data analysis, a least-square fit analysis was performed by using Voigt functions.

3 | RESULTS AND DISCUSSION

For the analysis of the electrode/electrolyte interface, we employ AuNP coated with SiO_2 (Au@SiO_2). Based on TEM images, the AuNP possess an average diameter of 53 nm, whereas the thickness of the SiO_2 layer ranges between 5 and 34 nm (average: 29 nm). A TEM image of Au@SiO_2 nanoparticles employed in this study is shown in the left panel of Figure 2 (see inset).

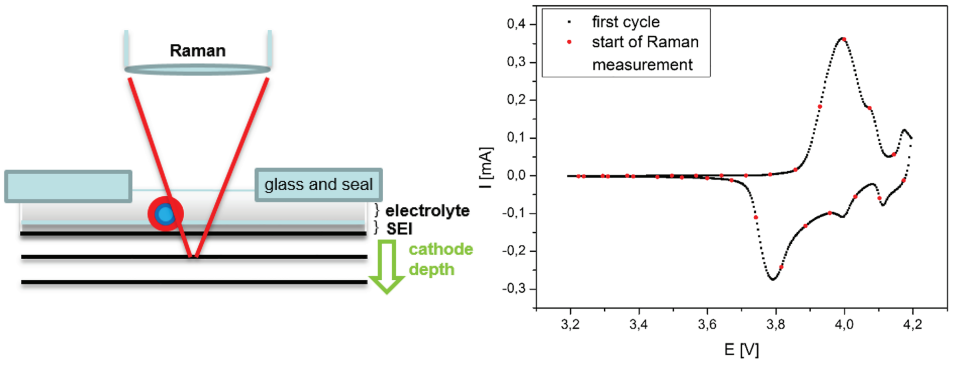

FIGURE 1 Left: In situ Raman spectroscopic analysis (632 nm) in the presence of Au@SiO_2 particles. Right: CV curve for the first cycle of the $LiCoO_2$ composite cathode. Metallic Li served as counter electrode and LP30 as electrolyte. Red points indicate the starting time of Raman measurements during cycling

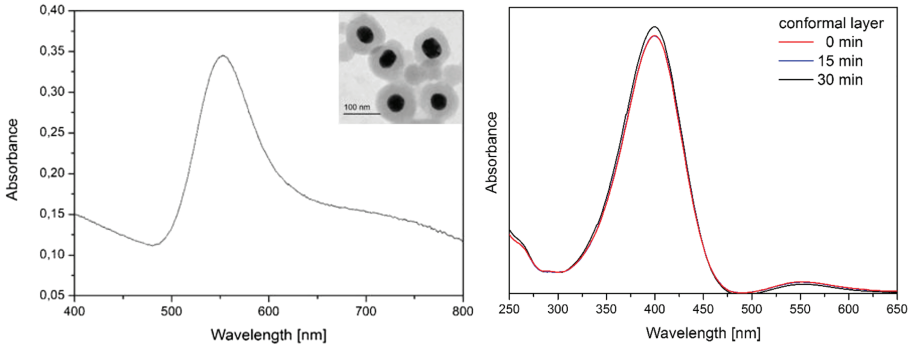

FIGURE 2 Left: UV–VIS spectrum of Au@SiO_2 solution. Inset: TEM image of Au@SiO_2 nanoparticles. Right: UV–VIS spectra of a *p*-nitrophenol solution with Au@SiO_2 particles used for the study

The UV–VIS spectrum of the coated AuNP is characterized by absorption between 500 and 600 nm (see Figure 2), due to localized surface plasmon resonance (LSPR) excitation. For details of the synthesis and characterization of the $Au@SiO_2$ nanoparticles, we refer to Section 2 and Figures S2 and S3.

To check whether the coated nanoparticles are inert, the gold-catalyzed reduction of *p*-nitrophenol was employed as an integral test reaction. For a nonconformal coating of the nanoparticles, the accessible gold catalyzes the reduction of *p*-nitrophenol to *p*-phenylenediamine, that is, the reduction of the nitro group, leading to a decrease of the absorption of the *p*-nitrophenol around 400 nm, and the appearance of product absorption at around 310 nm, as shown exemplarily in Figure S2.[32] No conversion of *p*-nitrophenol was observed for the $Au@SiO_2$ nanoparticles employed in this study, as shown in the right panel of Figure 2.

The distance between the AuNP and the sample is determined by the thickness of the SiO_2 layer. The dependence of the surface-enhanced Raman signal on layer thickness was determined by Li et al. on the basis of the pyridine signal, which decreases with increasing layer thickness.[25] For a layer thickness of more than 10 nm, no signal enhancement was reported. We therefore assume those $Au@SiO_2$ particles with smaller layer thicknesses to contribute more strongly to the Raman intensity.

In the following, we will discuss the Raman spectra of the $LiCoO_2$ cathode material, first in the absence and then in the presence of $Au@SiO_2$ nanoparticles. The left panel of Figure 3 depicts the ex situ Raman spectrum of an as prepared $LiCoO_2$ composite cathode (yellow line), which is characterized by Raman bands of $LiCoO_2$ and carbon black. The Raman-active modes of $LiCoO_2$ result in signals at 486 (E_g) and 597 cm^{-1} (A_{1g}).[31,34] The broad bands at around 1340 and 1600 cm^{-1} originate from carbon black in the composite cathode and are attributed to the defect band (D) and to the C—C stretching mode of graphite (G), respectively.[31] The additive PVDF of the composite cathode does not give a contribution to the Raman spectrum of the as prepared cathode, as evidenced by comparison with the spectrum of bare PVDF (see Figure S4).

The $LiCoO_2$ composite cathode containing $Au@SiO_2$ nanoparticles is characterized by the red spectrum in Figure 3. Resembling the spectrum without $Au@SiO_2$ (yellow spectrum), Raman bands of $LiCoO_2$ and carbon black are detected. Please note that no additional signals are observed due to the presence of $Au@SiO_2$ particles, the additive PVDF of the composite cathode, or from any of the precursor compounds ($LiNO_3$, $Co(NO_3)_2$, PVP, TEOS, SiO_2) (see Figures S5–S7).

In the presence of the electrolyte (LP30), additional electrolyte related Raman signals appear besides the $LiCoO_2$ and carbon related features (see black spectrum).

*[35] The green spectrum recorded after six CV cycles at a rate of 0.3 mV/s is dominated by electrolyte signals. After cycling, no Raman features of the cathode material and carbon black are detected, which is attributed to the overall decrease in sensitivity in the presence of the electrolyte and the heterogeneity of the composite cathode, displaying a rearrangement on the surface of the composite cathode. In fact, comparison of Raman maps of $LiCoO_2$ composite cathode before and after electrochemical cycling shows a redistribution of the chemical composition, due to a rearrangement of carbon additives, as described earlier.[31,36]

Interestingly, upon cycling, changes are observed at around 1090 cm^{-1}, as can be seen more clearly in the right panel of Figure 3. Based on a comparison with the spectrum of bare Li_2CO_3 (see Figures S8 and S9), we attribute the observed feature at 1090 cm^{-1} to the symmetric stretching vibration of carbonate in Li_2CO_3.[25,37] As

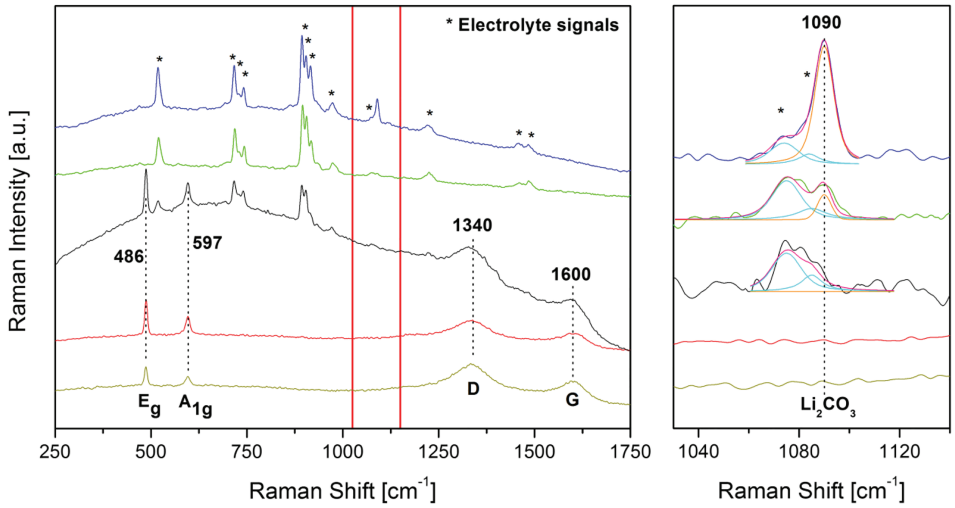

FIGURE 3 Left: Ex situ (yellow) Raman spectra of a $LiCoO_2$ composite cathode (84% $LiCoO_2$, 8% PVDF, 8% carbon black) and of a $LiCoO_2$ composite cathode with $Au@SiO_2$ particles (red) and quasi in situ Raman spectra of a cathode as assembled (black) and cycled (green). The blue spectrum corresponds to Li_2CO_3 and electrolyte (LP30) in the test cell without $Au@SiO_2$ particles. Right: Detailed view of the carbonate region of the Raman spectra (marked red in the left panel) after background subtraction together with the results of a fit analysis. Spectra were offset for clarity. Raman spectra were recorded with a 632 nm laser

will discussed below, the presence of Li_2CO_3 indicates the formation or deposition of Li_2CO_3 on the composite cathode. As shown in the enlarged view of Figure 3, the presence of Li_2CO_3 is further supported by comparison with the Raman spectrum of a mixture of Li_2CO_3 and electrolyte (LP30) (see blue spectrum). Please note that the EC electrolyte possesses Raman signals at 1075 and 1085 cm^{-1}.[35,38,39] Thus, for a detailed analysis of this spectral region, all contributions need to be taken into account (see below). Nevertheless, our results strongly suggest the formation of Li_2CO_3 as a component of the SEI after cycling and subsequent Raman analysis under quasi in situ conditions, that is, without exposure to air.

To enhance the understanding of the dynamic behavior of Li_2CO_3 as a component of the SEI, in situ SERS was applied directly under electrochemical conditions. Figure 4 depicts in situ Raman spectra of the $LiCoO_2$ composite cathode with Au@SiO_2 particles during the first discharging process in the range of 3.4 to 3.2 V and the second charging process in the range of 3.2 to 3.4 V. The full series of in situ Raman spectra during electrochemical cycling is provided in the Supporting information (see Figures S10–S12). The spectra are dominated by the Raman signals of the cathode and the electrolyte. During the discharge, the cathode is intercalated, and the E_g signal of $LiCoO_2$ increases. Additionally, as shown in the right panel of Figure 4, a dynamic behavior of the Li_2CO_3 signal at 1090 cm^{-1} is detected. The detailed view of the carbonate region of the Raman spectra shows the results of a least-square fit analysis of the carbonate Raman signal at 1090 cm^{-1} (orange) and Raman signals of EC (electrolyte) at 1085/1075 cm^{-1} (cyan) together with the resultant of all fit contributions (magenta). For details on the least-square fit analysis, please refer to Section 2. Initially, no Li_2CO_3 signal is observed during electrochemical cycling, but during discharging, the Li_2CO_3 signal emerges and declines during the subsequent charging process. Please note that Li_2CO_3 has neither been observed in the assembled state of the composite cathode (see Figure 3, black spectrum), nor after storage of the assembled battery (see Figure S13). The integrated Raman signals are depicted in Figure 5. The Raman signal of Li_2CO_3 increases during the first discharging cycle, reaches a maximum at 3.2 V, and during the second charging, decreases again (see Figures 4 and 5), until it disappears at 3.4 V. Beside the appearance of Li_2CO_3, no other additional Raman signals are observed during the in situ Raman measurements, for example, from Li_2O or LiOH (see Figures S8 and S14). Also, there is no indication for the formation of Co_3O_4, characterized by a signal at 691 cm^{-1},[40] suggesting degradation of $LiCoO_2$.[36]

In the following discussion, we address the formation and decomposition of Li_2CO_3, which may proceed via different reaction pathways. One possible scenario for Li_2CO_3 formation is induced by the reduction of EC and DMC, leading to the formation of lithium-alkyl compounds (see Equation 1). Li_2CO_3 may then be formed from $(CO_3Li)^-$ via reaction with Li^+ (see Equation 2).[8,10,11,41–43] Formation of Li_2CO_3 may also result from a reaction of intermediately formed Li_2O with CO_2 according to Equation 3.[26]

$$(CH_2O)_2CO + 2e^- + Li^+ \rightarrow C_2H_4 + (CO_3Li)^-, \quad (1)$$

$$(CO_3Li)^- + Li^+ \rightarrow Li_2CO_3, \quad (2)$$

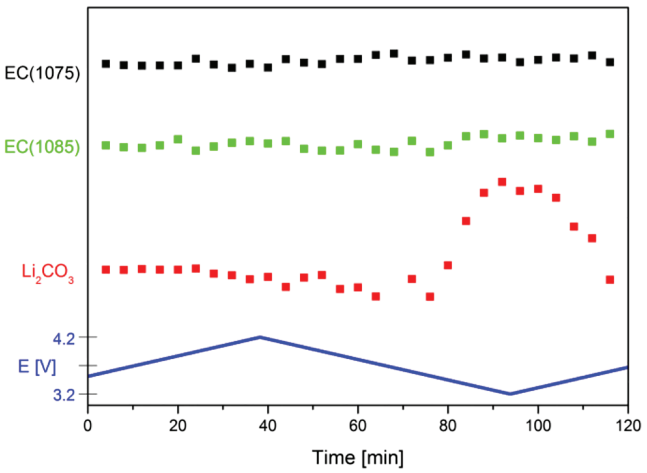

FIGURE 5 Integrated Raman signals of Li_2CO_3 (1090 cm^{-1}, red points) and EC (1085 cm^{-1}, green points, and 1075 cm^{-1}, black points) during the first charging, first discharging, and second charging process (blue line). The signals are the result of a least-square fit analysis of the spectra shown in Figures 4 and S8

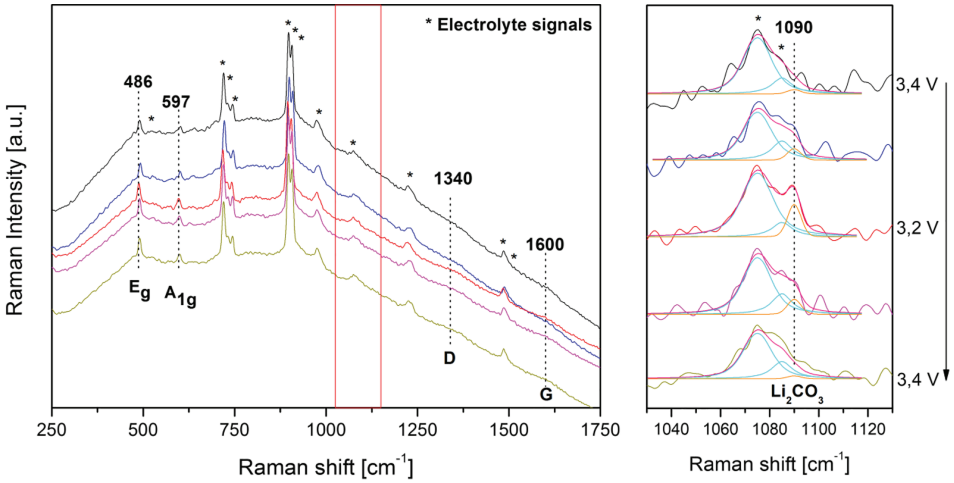

FIGURE 4 Left: In situ Raman spectra of a $LiCoO_2$ composite cathode (84% $LiCoO_2$, 8% PVDF, 8% carbon black) with Au@SiO_2 nanoparticles during the first discharging and second charging process using 632 nm laser excitation. Right: Detailed view of the carbonate region of the Raman spectra after background subtraction together with the results of a least-square fit analysis. Spectra were offset for clarity

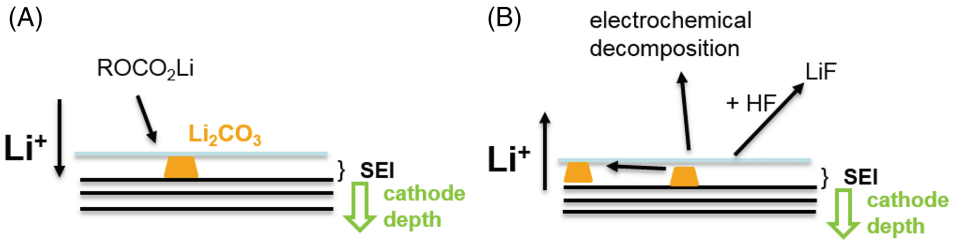

FIGURE 6 Proposed pathways for (A) Li_2CO_3 formation during discharging and (B) Li_2CO_3 decomposition during charging. Li_2CO_3 formation is based on lithium-alkyl compounds, while Li_2CO_3 decomposition proceeds via reaction with HF and/or electrochemical decomposition. A decline of the carbonate Raman signal due to surface rearrangement during electrochemical cycling cannot be excluded

$$Li_2O + CO_2 \rightarrow Li_2CO_3. \quad (3)$$

Furthermore, it has been shown that traces of water can produce LiOH (see Equation 4) and as a result of follow-up reactions Li_2O (see Equation 5) and Li_2CO_3 (see Equation 6).[6] Finally, CO_2 formed at the beginning of discharging may also react to Li_2CO_3 (see Equation 7).[6,44]

$$\text{Trace}\, H_2O + e^- + Li^+ \rightarrow LiOH + 1/2H_2, \quad (4)$$

$$LiOH + e^- + Li^+ \rightarrow Li_2O + 1/2H_2, \quad (5)$$

$$(CH_2OCO_2Li)_2 + H_2O \rightarrow Li_2CO_3 + CO_2 + (CH_2OH)_2, \quad (6)$$

$$2CO_2 + 2e^- + 2Li^+ \rightarrow Li_2CO_3 + CO. \quad (7)$$

The Raman spectra discussed above provide evidence for the formation of Li_2CO_3, while no signals from LiOH or Li_2O are detected. Based on these in situ spectroscopic results, we associate the observed Li_2CO_3 with the decomposition of lithium-alkyl compound, in contrast to previous proposals based on ex situ experiments, underlining the importance of direct analysis under electrochemical conditions.

Previously, Hy et al. observed the formation of Li_2CO_3 on LLNMO cathodes during discharging, while Li_2O was detected intermediately during charging.[26] It was proposed that LLNMO materials release oxygen to form Li_2O by charge compensation via a combination of $Ni^{2+/4+}$ and $Mn^{3+/4+}$ redox couples. While the authors applied a similar approach to prepare the composite cathode using carbon black and PVDF, they employed a graphite anode as counter electrode and 1 M $LiPF_6$ in EC/DEC (ratio 1:1) as electrolyte. Besides, Teshager et al. reported the formation of Li_2CO_3 on $LiCoO_2$ cathodes during charging above 4.0 V and during discharging below 3.6 V.[28] To explain their results, the authors proposed the decomposition of the EC electrolyte. In this context, it should be mentioned that the signals assigned to Li_2CO_3 in Teshager et al.[28] are different to those published previously by the same group.[45] In addition, the charging potential of 4.5 V was above the electrochemical window (<4.3 V) of the electrolyte and cathode, and the circulation of electrolyte differed from a diffusive behavior of a conventional battery under working conditions, thus making a direct comparison difficult.

Hong et al. observed FTIR signals of Li_2CO_3 appearing and disappearing repeatedly with discharging and charging on Li-excess metal oxides ($Li_{1.2}Ni_{0.2}Mn_{0.6}O_2$).[44] According to the authors, Li_2CO_3 is formed during discharging and decomposed to CO and CO_2 during charging, as supported by differential electrochemical mass spectroscopy (DEMS) during the charging steps. As HF may be present in the electrolyte due to impurities or $LiPF_6$ decomposition, a further Li_2CO_3 decomposition pathway is the reaction with HF, leading to LiF formation (see Equation 8).[44]

$$2HF + Li_2CO_3 \rightarrow 2LiF + H_2O + CO_2 \quad (8)$$

According to Bi et al., Li_2CO_3 may also undergo a chemical reaction with $LiPF_6$,[46] which besides LiF results in the formation of gaseous products (POF_3, CO_2), but due to its chemical nature, this process is not considered as pathway for Li_2CO_3 decomposition in the context of our results.

The proposed pathway of the composition/decomposition of Li_2CO_3 on a $LiCoO_2$ composite cathode is illustrated in Figure 6. Based on our spectroscopic findings, we propose a reaction pathway for the formation of Li_2CO_3, which is based on lithium-alkyl compounds formed from EC/DMC reduction. Li_2CO_3 decomposition may proceed via several pathways as discussed above, for example, by further reaction to LiF, and/or electrochemical decomposition to CO and CO_2. In contrast to the results by Hy et al. for LLNMO materials,[26] our Raman results show that for $LiCoO_2$ composite cathodes, other reaction pathways are operative during formation/decomposition of Li_2CO_3, highlighting the role of the cathode composition. In fact, our findings strongly suggest that the SEI formation originates from electrolyte decomposition. On the other hand, in the presence of Ni or Mn, the cathode material appears to be more reactive than $LiCoO_2$, thus opening different reaction pathways.

4 | CONCLUSIONS

To increase the sensitivity of in situ Raman spectroscopy for monitoring Li-ion batteries under working conditions, SERS was applied by using coated AuNP. AuNP were prepared starting from gold chloric acid, coated with SiO_2 ($Au@SiO_2$), and checked for conformity by a gold-catalyzed test reaction.

Ex situ and quasi in situ Raman spectra of cycled $LiCoO_2$ composite cathodes, recorded in the presence of $Au@SiO_2$ nanoparticles,

showed a carbonate signal at 1090 cm^{-1}, besides the signals of the active material ($LiCoO_2$) and the electrolyte, indicating the formation of Li_2CO_3. Raman experiments under working conditions confirm the formation of Li_2CO_3 during electrochemical cycling. Detailed analysis reveals the formation and decomposition of Li_2CO_3, highlighting its role as an intermediate of the SEI. The formation of Li_2CO_3 is proposed to proceed via electrolyte reduction. The disappearance of the Li_2CO_3 signal may occur via different pathways, for example, by reaction to LiF, or electrochemical decomposition, and may also proceed via rearrangement on the surface of the cathode. Our results indicate that Li_2CO_3 is an intermediate and a component of the SEI on a $LiCoO_2$ composite cathode. Thus, our analysis of the $LiCoO_2$ composite cathode demonstrates the potential of in situ/*operando* Raman spectroscopy to provide new insight into the SEI formation during operation of Li-ion batteries.

The dynamical aspects of the SEI are highly relevant to the discussion of electrode degradation. To extend the knowledge gained for $LiCoO_2$ composite cathodes, as a next step, the Raman approach could be applied to more complex cathode materials of NMC type. To further enhance the understanding of the SEI formation on cathode materials, it would also be interesting to systematically introduce Mn and Ni to the composite cathodes, exchanging Co with Mn and/or Ni, in the future.

ACKNOWLEDGMENTS

This work was supported by the Deutsche Forschungsgemeinschaft (DFG, HE 4515/8-1). The authors thank Dr. S. Lauterbach from the group of Prof. Dr. H.-J. Kleebe (TU Darmstadt) for performing the TEM measurements. Open Access funding enabled and organized by Projekt DEAL.

CONFLICT OF INTEREST

The authors declare no competing financial interest.

ORCID

Christian Hess https://orcid.org/0000-0002-4738-7674

ENDNOTE

* By comparison of the Raman signals of the electrolyte from the black spectrum in the presence of $Au@SiO_2$ nanoparticles and the blue spectrum in the absence of $Au@SiO_2$ nanoparticles (see Figure 2), no shift of the Raman signals of the electrolyte is observed due to adsorption on bare gold particles. This is a further indication of the conformity of the $Au@SiO_2$ particles.[35]

REFERENCES

1. Etacheri V, Marom R, Elazari R, Salitra G, Aurbach D. Challenges in the development of advanced Li-ion batteries: a review. *Energ Environ Sci*. 2011;4(9):3243-3262. doi:10.1039/c1ee01598b
2. Antolini E. $LiCoO_2$: formation, structure, lithium and oxygen nonstoichiometry, electrochemical behaviour and transport properties. *Solid State Ion*. 2004;170(3-4):159-171. doi:10.1016/j.ssi.2004.04.003
3. Hausbrand R, Cherkashinin G, Ehrenberg H, et al. Fundamental degradation mechanisms of layered oxide Li-ion battery cathode materials: methodology, insights and novel approaches. *Mater Sci Eng B*. 2015;192:3-25. doi:10.1016/j.mseb.2014.11.014
4. Vetter J, Novák P, Wagner MR, et al. Ageing mechanisms in lithium-ion batteries. *J Power Sources*. 2005;147(1-2):269-281. doi:10.1016/j.jpowsour.2005.01.006
5. Tripathi AM, Su W-N, Hwang BJ. *In situ* analytical techniques for battery interface analysis. *Chem Soc Rev*. 2018;47(3):736-851. doi:10.1039/C7CS00180K
6. Aurbach D. Review of selected electrode-solution interactions which determine the performance of Li and Li ion batteries. *J Power Sources*. 2000;89(2):206-218. doi:10.1016/S0378-7753(00)00431-6
7. Edström K, Gustafsson T, Thomas JO. The cathode-electrolyte interface in the Li-ion battery. *Electrochim Acta*. 2004;50(2-3):397-403. doi:10.1016/j.electacta.2004.03.049
8. Aurbach D, Zinigrad E, Cohen Y, Teller H. A short review of failure mechanisms of lithium metal and lithiated graphite anodes in liquid electrolyte solutions. *Solid State Ion*. 2002;148(3-4):405-416. doi:10.1016/S0167-2738(02)00080-2
9. Peled E, Menkin S. Review—SEI: past, present and future. *J Electrochem Soc*. 2017;164(7):A1703-A1719. doi:10.1149/2.1441707jes
10. Aurbach D, Zaban A, Gofer Y, et al. Recent studies of the lithium-liquid electrolyte interface electrochemical, morphological and spectral studies of a few important systems. *J Power Sources*. 1995;54(1):76-84. doi:10.1016/0378-7753(94)02044-4
11. Aurbach D, Markovsky B, Levi MD, et al. New insights into the interactions between electrode materials and electrolyte solutions for advanced nonaqueous batteries. *J Power Sources*. 1999;81:95-111. doi:10.1016/S0378-7753(99)00187-1
12. Verma P, Maire P, Novák P. A review of the features and analyses of the solid electrolyte interphase in Li-ion batteries. *Electrochim Acta*. 2010;55(22):6332-6341. doi:10.1016/j.electacta.2010.05.072
13. Baddour-Hadjean R, Pereira-Ramos J-P. Raman microspectrometry applied to the study of electrode materials for lithium batteries. *Chem Rev*. 2010;110(3):1278-1319. doi:10.1021/cr800344k
14. Palacin MR. Recent advances in rechargeable battery materials: a chemists perspective. *Chem Soc Rev*. 2009;38(9):2565-2575. doi:10.1039/b820555h
15. Reimers JN, Dahn JR. Electrochemical and *in situ* X-ray diffraction studies of lithium intercalation in Li_xCoO_2. *J Electrochem Soc*. 1992;139(8):2091-2097. doi:10.1149/1.2221184
16. Inaba M, Iriyama Y, Ogumi Z, Todzuka Y, Tasaka A. Raman study of layered rock-salt $LiCoO_2$ and its electrochemical lithium deintercalation. *J Raman Spectrosc*. 1997;28(8):613-617. doi:10.1002/(SICI)1097-4555(199708)28:8<613::AID-JRS138>3.0.CO;2-T
17. Anema JR, Li J-F, Yang Z-L, Ren B, Tian Z-Q. Shell-isolated nanoparticle-enhanced raman spectroscopy: expanding the versatility of surface-enhanced Raman scattering. *Annu Rev Anal Chem*. 2011;4(1):129-150. doi:10.1146/annurev.anchem.111808.073632
18. Fleichschmann M, Hendra PJ, McQuillan AJ. Raman spectra of pyridine adsorbed at a silver electrode. *Chem Phys Lett*. 1974;26(2):163-166. doi:10.1016/0009-2614(74)85388-1
19. Stiles PL, Dieringer JA, Shah NC, Van Duyne RP. Surface-enhanced Raman spectroscopy. *Annu Rev Anal Chem*. 2008;1(1):601-626. doi:10.1146/annurev.anchem.1.031207.112814
20. Sharma B, Frontiera RR, Henry A-I, Ringe E, Van Duyne RP. SERS: materials, applications, and the future. *Mater Today*. 2012;15(1–2):16-25. doi:10.1016/S1369-7021(12)70017-2
21. Flood AH, Stoddart JF, Steuerman DW, Heath JR. Whence molecular electronics. *Science*. 2004;306(5704):2055-2056. doi:10.1126/science.1106195
22. Olson MA, Botros YY, Stoddart JF. Mechanostereochemistry. *Pure Appl Chem*. 2010;82(8):1569-1574. doi:10.1351/PAC-CON-10-02-09
23. Van Duyne RP, Haushalter JP. Resonance Raman spectroelectrochemistry of semiconductor electrodes: the

photooxidation of tetrathiafulvalene at n-GaAs(100) in acetonitrile. *J Phys Chem*. 1984;88(12):2446-2451. doi:10.1021/j150656a006
24. Paxton WF, Kleinman SI, Basuray AN, Stoddart JF, Van Duyne RR. Surface-enhanced Raman spectroelectrochemistry of TTF-modified self-assembled monolayers. *J Phys Chem Lett*. 2011;2(10):1145-1149. doi:10.1021/jz200523q
25. Li JF, Huang YF, Ding Y, et al. Shell-isolated nanoparticle-enhanced Raman spectroscopy. *Nature*. 2010;464(7287):392-395. doi:10.1038/nature08907
26. Hy S, Felix F, Rick J, Su W-N, Hwang BJ. Direct *in situ* observation of Li_2O evolution on Li-rich high-capacity cathode material, $Li[Ni_xLi_{(1-2x)/3}Mn_{(2-x)/3}]O_2$ ($0 \le x \le 0.5$). *J Am Chem Soc*. 2014;136(3):999-1007. doi:10.1021/ja410137s
27. Hy S, Felix F, Chen Y-H, Liu J-Y, Rick J, Hwang B-J. *In situ* surface enhanced Raman spectroscopic studies of solid electrolyte interphase formation in lithium ion battery electrodes. *J Power Sources*. 2014;256:324-328. doi:10.1016/j.jpowsour.2014.01.092
28. Teshager MA, Lin SD, Hwang B-J, Wang F-M, Hy S, Haregewoin AM. In situ DRIFTS analysis of solid-electrolyte interphase formation on Li-rich $Li_{1.2}Ni_{0.2}Mn_{0.6}O_2$ and $LiCoO_2$ cathodes during oxidative electrolyte decomposotion. *ChemElectroChem*. 2016;3(2):337-345. doi:10.1002/celc.201500290
29. Galloway TA, Cabo-Fernandez L, Aldous IM, Braga F, Hardwick LJ. Shell isolated nanoparticles for enhanced Raman spectroscopy studies in lithium-oxygen cells. *Faraday Disc*. 2017;205:469-490. doi:10.1039/C7FD00151G
30. Pechini PM Method of preparing lead and alkaline earth titanates and niobates and coating method using the same to form a capacitor. US Patent Nr. 3.330.697, 1967.
31. Gross T, Hess C. Raman diagnostics of $LiCoO_2$ electrodes for lithium-ion batteries. *J Power Sources*. 2014;256:220-225. doi:10.1016/j.jpowsour.2014.01.084
32. Zhao Y, Yang D, Hu H, et al. A simple approach to the synthesis of eccentric Au@SiO_2 janus nanostructures and their catalytic applications. *Surf Sci*. 2016;648:313-318. doi:10.1016/j.susc.2015.10.044
33. Radtke M, Hess C. Operando Raman shift replaces current in electrochemical analysis of Li-ion batteries: a comparative study. *Molecules*. 2021;26(15):4667. doi:10.3390/molecules26154667
34. Heber M, Hofmann K, Hess C. Raman diagnostics of cathode materials for Li-ion batteries using multi-wavelength excitation. *Batteries*. 2022;8(2):10. doi:10.3390/batteries8020010
35. Yang G, Ivanov IN, Ruther RE, et al. Electrolyte solvation structure at solid-liquid interface probed by nanogap surface-enhanced Raman spectroscopy. *ACS Nano*. 2018;12(10):10159-10170. doi:10.1021/acsnano.8b05038
36. Gross T, Hess C. Spatially-resolved in situ Raman analysis of $LiCoO_2$ electrodes. *ECS Trans*. 2014;63(12):137-144. doi:10.1149/06112.0001ecst
37. Koura N, Kohara S, Takeuchi K, et al. Alkali carbonates: Raman spectroscopy, ab initio calculations, and structure. *J Mol Struct*. 1996;382(3):163-169. doi:10.1016/0022-2860(96)09314-3
38. Fortunato B, Mirone P, Fini G. Infrared and Raman spectra and vibrational assignment of ethylene carbonate. *Spectrochim Acta A Mol Biomol Spectrosc*. 1971;27A(9):1917-1927. doi:10.1016/0584-8539(71)80245-3
39. Chen D, Mahmoud MA, Wang J-H, et al. Operando investigation into dynamic evolution of cathode-electrolyte interfaces in a Li-ion battery. *Nano Lett*. 2019;19(3):2037-2043. doi:10.1021/acs.nanolett.9b00179
40. Hadjiev VG, Iliev MN, Vergilov IV. The Raman spectra of Co_3O_4. *J Phys C: Solid State Phys*. 1988;21(7):L199-L201. doi:10.1088/0022-3719/21/7/007
41. Wang Y, Nakamura S, Ue M, Balbuena PB. Theoretical studies to understand surface chemistry on carbon anodes for lithium-ion batteries: reduction mechanisms of ethylene carbonate. *J Am Chem Soc*. 2001;123(47):11708-11718. doi:10.1021/ja0164529
42. Herstedt M, Abraham DP, Kerr JB, Edström K. X-ray photoelectron spectroscopy of negative electrodes from high-power lithium-ion cells showing various levels of power fade. *Electrochim Acta*. 2004;49(28):5097-5110. doi:10.1016/j.electacta.2004.06.021
43. Dedryvère R, Martinez H, Leroy S, et al. Surface film formation on electrodes in a $LiCoO_2$/graphite cell: a step by step XPS study. *J Power Sources*. 2007;174:462-468.
44. Hong J, Lim H-D, Lee M, et al. Critical role of oxygen evolved from layered Li-excess metal oxides in lithium rechargeable batteries. *Chem Mater*. 2012;24(14):2692-2697. doi:10.1021/cm3005634
45. Haregewoin AM, Shie T-D, Lin SD, Hwang B-J, Wang F-M. An effective in situ DRIFTS analysis of the solid electrolyte interface in lithium-ion battery. *ECS Trans*. 2013;53(36):23-32. doi:10.1149/05336.0023ecst
46. Bi Y, Wang T, Liu M, et al. Stability of Li_2CO_3 in cathode of lithium ion battery and its influence on electrochemical performance. *RSC Adv*. 2016;6(23):19233-19237. doi:10.1039/C6RA00648E

SUPPORTING INFORMATION

Additional supporting information may be found in the online version of the article at the publisher's website.

How to cite this article: Heber M, Hess C. Monitoring electrode/electrolyte interfaces of Li-ion batteries under working conditions: A surface-enhanced Raman spectroscopic study on $LiCoO_2$ composite cathodes. *Surf Interface Anal*. 2022;54(8):847-854. doi:10.1002/sia.7097